MAGNETORHEOLOGICAL ELASTOMER ISOLATOR IN COMPRESSION MODE
FOR IMU VIBRATION ISOLATION

Yang Fufeng and Tao Yu

msp

MAGNETORHEOLOGICAL ELASTOMER ISOLATOR IN COMPRESSION MODE FOR IMU VIBRATION ISOLATION

YANG FUFENG AND TAO YU

Magnetorheological elastomer (MRE) is a new class of smart materials, whose mechanical properties can be continuously and rapidly controlled by an applied magnetic field. A compression MRE isolator was designed and fabricated. The mechanical tests were conducted by instron. The dynamic properties of MRE isolator were studied by frequency sweeping tests, using vibration table under 1 g acceleration excitation with different currents. The peak value of the transmissibility was decreased by 29.7% and the natural frequency of the single degree of freedom (SDOF) system approximately increased by 18.54% while the current varied from 0.0 A to 4.0 A. Moreover, the equivalent stiffness and damping coefficients were identified from experimental data. In order to further evaluate the effectiveness of MRE isolator for vibration control, the SDOF inertial measurement unit (IMU) isolation system was simulated under random vibration conditions. The peak acceleration of power spectral density (PSD) was decreased by 48.8% when applying a series of constant currents. The study verifies that the compression MRE isolator is capable of increasing system stiffness, changing system natural frequency and decreasing system vibration.

1. Introduction

Vibration isolation is the most popular structures protection technique for many engineering structures. However, research has revealed that the traditional passive vibration isolation systems, due to the passive nature, are inable to adapt to changes in structural parameters over time, which results in reduced performance. Any changes of the mechanical system such as varying mass or uncertain external excitations and disturbances are not well supported by a passive isolation system. A great deal of efforts have been dedicated to improve the performance of the traditional passive vibration isolation system. A series of research efforts have been made for the development of novel adaptive vibration isolators utilizing magnetorheological elastomers (MREs) [Brancati et al. 2017; Tao et al. 2019; Yang et al. 2016]. MRE is a type of smart rubber, generally fabricated by dispersing magnetized particles in a solid polymer medium such as natural rubber and curing under an applied magnetic field, which causes the magnetic particles to align in chains. The elastic modulus or stiffness of MRE increases monotonically with the applied magnetic field. This unique and controllable stiffness property of MREs offers a great opportunity for the development of adaptive vibration isolators [Liao et al. 2012; Behrooz et al. 2014]. The tunable automotive mounts and bushings based on MRE were developed in [Ginder et al. 2000]. They found that the suspension resonances excited by torque variation could be suppressed by shifting the resonance away from the excitation frequency. Another similar adaptive tuned vibration buffer based on MRE was studied in [Deng et al. 2006]. MRE are currently being researched by many industries including the
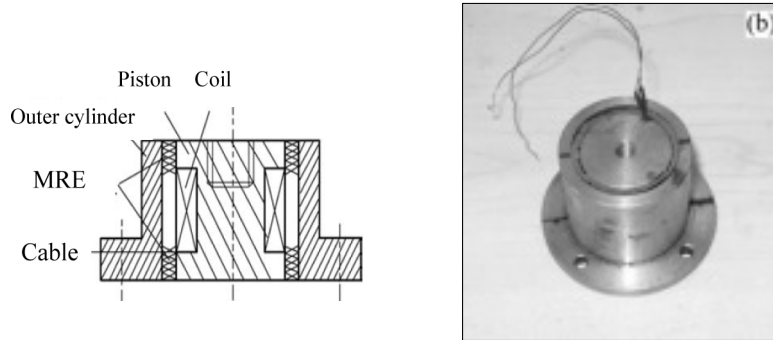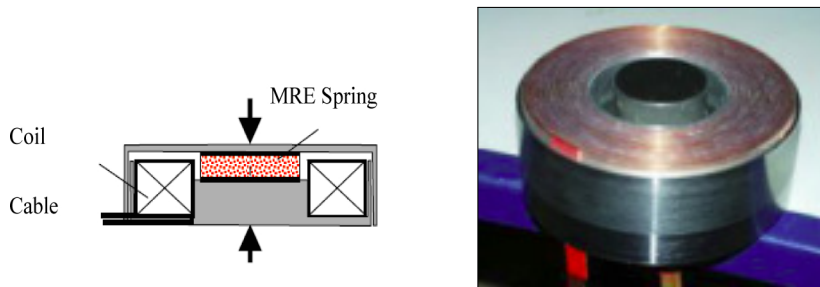
**Figure 1.** Schematic configuration and photograph of MRE with shear deformation [Dong et al. 2009].

Figure 2. Schematic configuration and photograph of MRE with compression deformation [Kallio 2005].

automotive, building, and space industries. Such as, space applications include isolation of payloads from rocket stages during launch and isolation of mirrors in space telescopes.

There is a wide variety of non-magnetic matrices of MREs, like natural rubbers, silicone rubbers and polyurethanes with a varying filler volume fraction. MREs can be classified into two types: isotropic and anisotropic. Isotropic MRE is a homogeneous mixture of host matrix and magnetic particles. Anisotropic MRE is fabricated by aligning the magnetic particles into a chain-like structure when cured with an applied magnetic field. Under the influence of a magnetic field the MRE becomes stiffer due to decreased distance between the magnetic particles. The effect is usable for the applications of vibration isolation. The MRE magnetostrictive effect is the most important feature for the vibration control application. Shearing of the cured composite in the presence of a magnetic field causes MRE work dependent shear modulus. Aligned MREs are shown to have a field dependent shear modulus, but the other elastic properties are still quite unexplored, especially when the MREs are measured without the applied magnetic field. As shown in Figure 1, the shear deformation of MRE appears by the motion of the piston. The magnetic field exists in the MRE which is perpendicular to the motion of the piston after the current is applied to the coil [Dong et al. 2009].

As the same, aligned MREs are shown to have a field dependent compression modulus. As shown in Figure 2, the magnetic field in the MRE spring element is along the same direction as its cylinder axis (in the chain direction of aligned MREs) during the compression tests [Kallio 2005].
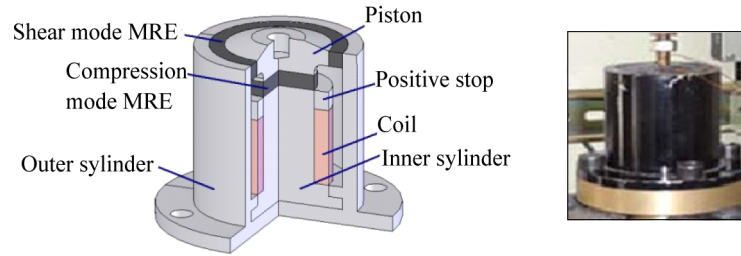
Figure 3. Magnetorheological elastomer isolator in shear-compression mixed mode [Liu 2012].

Figure 3 shows a magnetorheological elastomer isolator working in shear-compression mixed mode, which is composed of two pieces of MREs, one works in shear mode and another works in compression mode. Excitation magnetic field of the isolator is generated by the excitation coil, its direction is parallel with the pressure direction and vertical with shear direction. As the modulus of MRE in compression mode is higher than that in shear mode, the structure can effectively reduce the static strain caused by the quality of the isolation device [Liu 2012].

In this study, a novel MRE isolator working in compression mode is proposed. The design, fabrication and tests of compression MRE isolator are introduced. The experimental study on the mechanical properties of MRE isolator is performed by instron and vibrating table, respectively. Then the compression force and displacement test results are presented and discussed. The stiffness and damping ratio coefficients are identified from frequency sweeping test data. The SDOF IMU isolator system with four MRE isolators is developed and simulated under random excitation input. The simulation results of PSD and displacement are discussed and the performance of MRE isolator is evaluated. The compression MRE isolator proposed in this paper can meet the requirements of the working environment and installation space for the IMU. It has the characteristics of small volume, integrated preparation and controllable output force.

2. Fabrication of the compression MRE isolator

The schematic design of the compression MRE isolator is shown in Figure 4. As can be seen, the design consists of a cylindrical MRE, two electromagnetic coils, two iron core connectors and an outer magneto-conductivity casing. The structure of isolator allows the MRE to work in compression mode. The motion of payload can be controlled in both up and down directions. The magnetic field is generated by the coils and controlled by tuning the current. Moreover, the direction of magnetic field in the MRE is parallel to the motion of the iron cores after the current is applied to the coils. One end of each iron core is embedded inside the MRE. The diameter of the MRE is 35 mm, and the diameter of the coil wire is 0.50 mm with a total winding number of 300 turns. Each coil has electric resistance of 1.38 Ω.

Natural rubber is a flexible, rubbery polymer obtained from the tree Hevea Brasiliensis. Natural rubber is a popular choice for the preparation of MRE because of its advantageous mechanical characteristics. The particles used are BASF EW carbonyl iron powders and the mass fraction of iron particles is 60%. A compound of the uncured rubber is accomplished on a laboratory scale two-roll mill. After the rubber is well mixed, the iron particles are introduced into the rubber again on the two-roll mill. After the final compounding, the MREs are prepared in electromagnetic mold, as shown in Figure 5. The mold
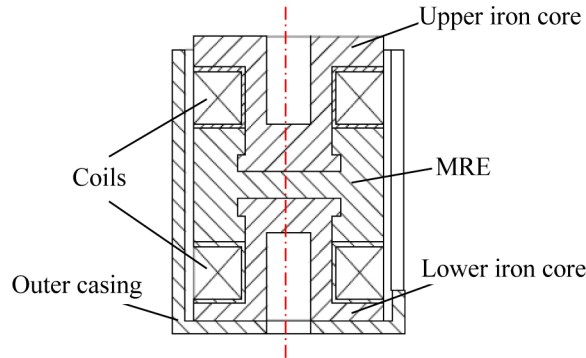
Figure 4. Schematic of the MRE isolator.
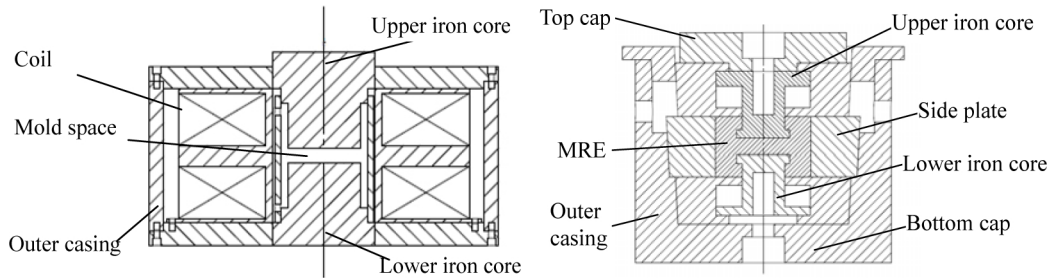
**Figure 5.** Schematic of the electromagnetic device (left) and the MRE mold (right).

Figure 6. Different assembly forms of MRE isolator: compound structure (left), compound structure with coils (middle), and complete structure (right).

is pre-heated in the vulcanizing machine, and the high pressure is applied to the polymer during the curing process. Current is applied to the electromagnet coils to produce the desired alignment magnetic field, with a magnetic induction of 1 Tesla. Natural rubber MREs are cured for 15 min before taken out. Figure 6 presents different assembly forms of MRE isolator. The compound structure is made up of MRE, magnetizers and coil skeletons.

3. Test and discussion

The quasi-static and dynamic tests are carried out to verify the performances of the MRE isolators and to obtain the relationship among stiffness, damping and current.

DC
power
electromagnetic device   instron
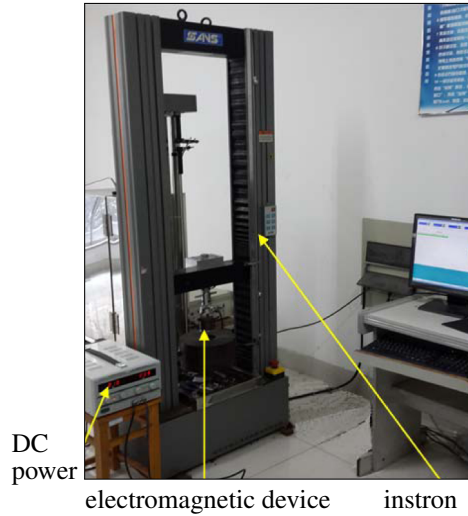
Figure 7. MRE experimental test setup.

3.1. *Compression force and displacement test.* The experimental study on the mechanical properties of the compound structure as shown in Figure 6(b) is performed. The purpose of the quasi-static tests is to evaluate and record the physical properties of MRE isolators under different magnetic fields and different displacement amplitudes. The experimental test setup is shown in Figure 7. MRE isolator is located in the electromagnetic device and connected to the instron (CMT-4254). DC power source provides current to the coils inside the electromagnetic device which generates the magnetic field surrounding the MRE isolators. And the magnetic field intensity is measured by magnetometer. Controlled compression displacement of the MRE isolator is supplied by the instron. The experiments are conducted with room temperature 25 °C and the loading rate 1 mm/Min. The compression force and displacement curves of the MRE are shown in Figure 8. It can be seen that the force of the MRE isolator increases as the increasement of applied magnetic field and displacement, respectively. The displacement is almost 0 mm when the static force of MRE isolator is about 20 N. It means that the static stiffness of MRE isolator is enough to support IMU and meet the installation conditions.
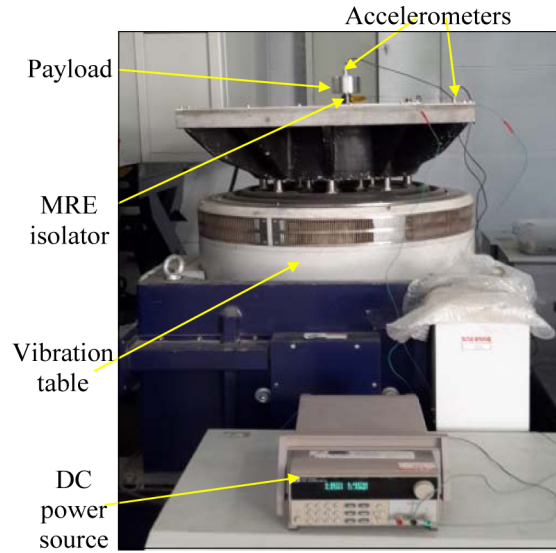
3.2. *Frequency sweeping test.* The MRE isolator is evaluated by the frequency sweeping test. It is carried out by a vibration table with 1g acceleration and different currents. The experimental setup of frequency sweeping test with MRE isolator is shown in Figure 9. The SDOF vibration system is composed of a payload and a MRE isolator. The payload of the SDOF system is supported by MRE isolator, which is mounted on the vibration table. The payload acceleration and vibration table input acceleration are measured by two accelerometers (PCB Model 352C33) respectively. DC power source provides current to the coils inside MRE isolator which generates the magnetic field surrounding the MRE. The parameters of the frequency sweeping test are as follows:

Sweep frequency: 20 Hz to 200 Hz   Payload: 2.0 kg   Acceleration: 1 g Current: 0, 1, 2, 3, 4 A

Figure 10 Experimental results with different currents shows the acceleration transmissibility results for a frequency range between 20–100 Hz and the acceleration amplitude of 1 g with different currents
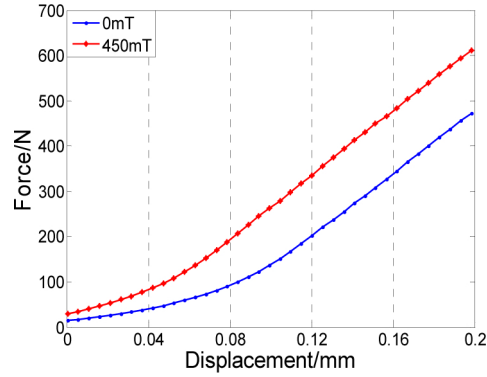
Figure 8. Compression force and displacement curves.

**Figure 9.** Experimental setup of frequency sweeping test with MRE isolator.

applied to the MRE isolator. As can been seen, the natural frequency of the SDOF system increases from 42.23 Hz at 0 A to 50.06 Hz at 4 A. The peak value of the transmissibility is reduced from 5.403 to 3.796. The natural frequency of the SDOF system approximate increase equals to 19.8%. The peak value has the total reduction of 29.7% in the acceleration transmissibility approximately.

3.3. *The identification of stiffness and damping ratio coefficients.* The stiffness and damping ratio coefficients are identified by using the experimental results of acceleration transmissibility as shown in Figure 10. The steps are listed as follows:
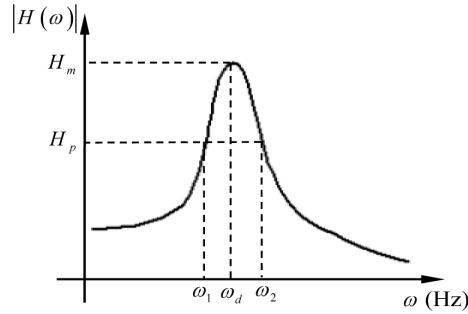
1) The peak value of the acceleration transmissibility is H_m, and it represents the value of half power point H_p. The relationship between them can be written as

$$H_p = \frac{H_m}{\sqrt{2}} \approx 0.707 H_m.$$ (1)
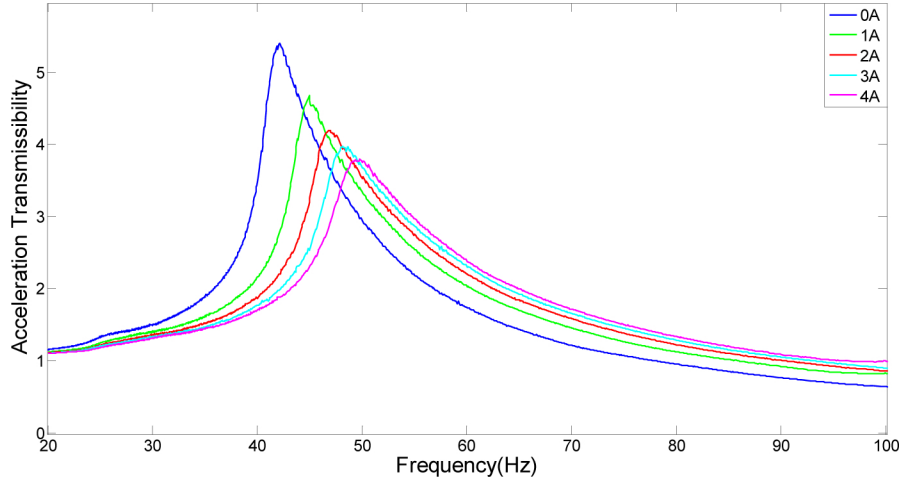
Figure 10. Experimental results with different currents.

Figure 11. Relation of half power points and frequency.

The frequencies ω_1 and ω_2 correspond to half power points of the acceleration transmissibility are shown in Figure 12, right. The coefficient is given by the equation

$$n = \frac{\omega_2 - \omega_1}{2}. \tag{2}$$

2) The resonance frequency ω_d can be obtained through the frequency response curve, and the natural frequency is given by

$$\omega_n = \sqrt{\omega_d^2 + n^2}. \tag{3}$$

The damping ratio is defined as

$$\zeta = n/\omega_n. \tag{4}$$

3) The stiffness of MRE isolator is calculated through the equation

$$k = 4\pi^2 \omega_n^2 m, \tag{5}$$

where m is the payload mass.

Table 1 lists the normalized equivalent stiffness and damping coefficients from experimental data. The maximum value of effective stiffness is 197.9 kN/m and the maximum increase of the effective stiffness

current	natural frequency	stiffness	damping ratio
0 A	42.23 Hz	140.8 kN/m	0.071
1 A	45.08 Hz	160.5 kN/m	0.080
2 A	47.03 Hz	174.6 kN/m	0.094
3 A	48.40 Hz	184.9 kN/m	0.103
4 A	50.06 Hz	197.9 kN/m	0.110

Table 1. Equivalent stiffness and damping coefficients of MRE isolator.

is 40.55% as current varies from 0.0 A to 4.0 A. The maximum increase of damping ratio is 54.9%. The test results reveal that as the applied magnetic field increases, the natural frequency, stiffness and damping ratio of the MRE isolator increase in value. The relationships of frequency (Hz), stiffness (kN/m), damping ratio and current (A), obtained by polynomial fitting, are as follows:

$$f(I) = 0.0229I^4 - 0.0842I^3 - 0.3579I^2 + 3.2692I + 42.23, \tag{6}$$

$$K(I) = 0.1958I^4 - 0.875\ I^3 - 1.5458I^2 + 21.925I + 140.8, \tag{7}$$

$$\zeta(I) = 0.0005I^4 - 0.0049I^3 + 0.0135I^2 - 0.0001I + 0.071. \tag{8}$$

4. Theoretical model and calculation method

The IMU usually works in the random vibration environment. The control relationships of the single MRE isolators are substituted into the dynamics simulation of IMU isolation system. Then the IMU output power spectrum under the typical random vibration environment is obtained. Thus, the aim of predicting the isolation effect of MRE isolators for IMU is achieved.

4.1. *Dynamics model of IMU system.* The dynamics model of IMU system is established as shown in Figure 12, left. According to the dynamics properties of IMU system, it is considered as a multibody system comprising rigid bodies, springs and dampers. The motion of the carrier 0 is the input of the IMU system. Platform 5 and three gyros 9∼11 are considered as rigid bodies, respectively; platform and carrier are linked by MRE isolators 1∼4, which are regarded as controlled spring-and-damper hinges longitudinally vibrating in space. The connections 6∼8 between platform and gyros are considered as spatial spring-and-damper hinges.

Isolators 1∼4 can be treated as one equivalent hinge element, which will be shown in the following, thus the dynamics model of IMU system can be dealt with a tree system. Its topology figure can be got easily as shown in Figure 12, right. In the topology figure, the circles represent body elements wherein the numbers indicate the corresponding body element number; the arrows denote hinge elements and the transfer directions of state vectors, the numbers aside are the sequence numbers of the hinge elements. The boundaries are all numbered as 0. The boundaries corresponding to elements 1∼4 are considered as output boundaries, and the boundaries corresponding to elements 9∼11 are considered as input boundaries. So the IMU isolation system is considered as a multibody system composed of 4 rigid bodies and 3 hinges.
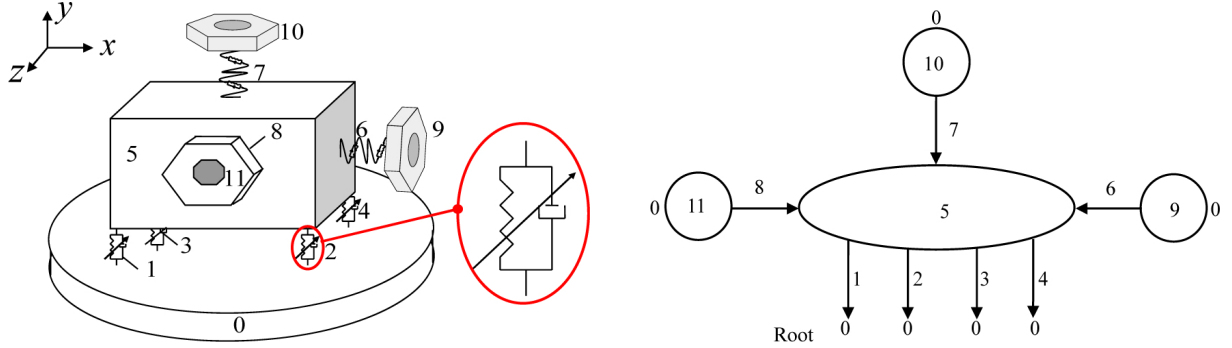
Figure 12. Left: dynamics model of laser IMU isolation system. Right: Topology of laser gyro SIMU system.

The state vectors of the input and output points of every element and the boundary points are defined as

$$\mathbf{Z} = \begin{bmatrix} X & Y & Z & \Theta_x & \Theta_y & \Theta_z & M_x & M_y & M_z & Q_x & Q_y & Q_z \end{bmatrix}^{\mathrm{T}} \tag{9}$$

The state variables in the state vector are the linear displacements, angular displacements, internal forces and internal torques in the modal coordinates. The specific derivation of the transfer matrix of one degree of freedom system can refer to reference [Chen et al. 2013].

4.2. *Transfer equation and transfer matrix of system components.*

Transfer equation and transfer matrix of elements 1∼4. Each MRE isolator is regarded as a spatial stiffness-and-damper hinge, which contains stiffness along the X, Y and Z directions. As four isolators are sandwiched between two rigid bodies, they can be treated as one new element, namely, an equivalent spring-and-damper hinge with single input end and single output end. The principal vectors and principal moments of the element at the output end and the input end are the same. We obtain

$$\begin{bmatrix} M_x \\ M_y \\ M_z \\ Q_x \\ Q_y \\ Q_z \end{bmatrix}_{\mathrm{O}} = \begin{bmatrix} M_x \\ M_y \\ M_z \\ Q_x \\ Q_y \\ Q_z \end{bmatrix}_{\mathrm{I}} = \mathbf{K}_{1-4} \begin{bmatrix} X \\ Y \\ Z \\ \Theta_x \\ \Theta_y \\ \Theta_z \end{bmatrix}_{\mathrm{O}} - \mathbf{K}_{1-4} \begin{bmatrix} X \\ Y \\ Z \\ \Theta_x \\ \Theta_y \\ \Theta_z \end{bmatrix}_{\mathrm{I}}, \quad \begin{bmatrix} X \\ Y \\ Z \\ \Theta_x \\ \Theta_y \\ \Theta_z \end{bmatrix}_{\mathrm{O}} = \begin{bmatrix} X \\ Y \\ Z \\ \Theta_x \\ \Theta_y \\ \Theta_z \end{bmatrix}_{\mathrm{I}} + \mathbf{K}_{1-4}^{-1} \begin{bmatrix} M_x \\ M_y \\ M_z \\ Q_x \\ Q_y \\ Q_z \end{bmatrix}_{\mathrm{I}}. \tag{10}$$

The transfer equation of elements 1∼4 is

$$\mathbf{Z}_{1\sim4,\mathrm{O}} = \mathbf{U}_{1\sim4}\mathbf{Z}_{1\sim4,\mathrm{I}}. \tag{11}$$

The transfer matrix is

$$\mathbf{U}_{1\sim4} = \begin{bmatrix} \mathbf{I}_6 & \mathbf{K}_{1\sim4}^{-1} \\ \mathbf{O}_{6\times6} & \mathbf{I}_6 \end{bmatrix}, \tag{12}$$

where

$$
K_{1\sim4} =
\begin{bmatrix}
0 & -\sum_{i=1}^{4} k_{yi}c_i & \sum_{i=1}^{4} k_{zi}b_i & \sum_{i=1}^{4}(k_{yi}c_i^2+k_{zi}b_i^2) & -\sum_{i=1}^{4} k_{zi}a_ib_i & -\sum_{i=1}^{4} k_{yi}a_ic_i \\
\sum_{i=1}^{4} k_{xi}c_i & 0 & -\sum_{i=1}^{4} k_{zi}a_i & -\sum_{i=1}^{4} k_{zi}b_ia_i & \sum_{i=1}^{4}(k_{xi}c_i^2+k_{zi}a_i^2) & -\sum_{i=1}^{4} k_{xi}b_ic_i \\
-\sum_{i=1}^{4} k_{xi}b_i & \sum_{i=1}^{4} k_{yi}a_i & 0 & -\sum_{i=1}^{4} k_{yi}c_ia_i & -\sum_{i=1}^{4} k_{xi}c_ib_i & \sum_{i=1}^{4}(k_{xi}b_i^2+k_{yi}a_i^2) \\
-\sum_{i=1}^{4} k_{xi} & 0 & 0 & 0 & -\sum_{i=1}^{4} k_{xi}c_i & \sum_{i=1}^{4} k_{xi}b_i \\
0 & -\sum_{i=1}^{4} k_{yi} & 0 & \sum_{i=1}^{4} k_{yi}c_i & 0 & -\sum_{i=1}^{4} k_{yi}a_i \\
0 & 0 & -\sum_{i=1}^{4} k_{zi} & -\sum_{i=1}^{4} k_{zi}b_i & \sum_{i=1}^{4} k_{zi}a_i & 0
\end{bmatrix}
$$

Here (a_i, b_i, c_i) $(i = 1\sim4)$ denote the positions of isolators $1\sim4$ on the carrier and platform, and (k_{xi}, k_{yi}, k_{zi}) are the initial stiffness coefficients of the isolators.

The transfer equation and transfer matrix of element 5. Platform 5 is considered as a rigid body with three input ends and single output end, and its transfer equation is

$$
\begin{cases}
\boldsymbol{Z}_{5,O} = \boldsymbol{U}_5\boldsymbol{Z}_{5,I_1} + \boldsymbol{U}_{5,I_2}\boldsymbol{Z}_{5,I_2} + \boldsymbol{U}_{5,I_3}\boldsymbol{Z}_{5,I_3}, \\
\boldsymbol{H}_5\boldsymbol{Z}_{5,I_1} = \boldsymbol{H}_{5,I_2}\boldsymbol{Z}_{5,I_2}, \\
\boldsymbol{H}_5\boldsymbol{Z}_{5,I_1} = \boldsymbol{H}_{5,I_3}\boldsymbol{Z}_{5,I_3}.
\end{cases} \tag{13}
$$

The transfer matrix is given by

$$
\boldsymbol{U}_5 =
\begin{bmatrix}
\boldsymbol{I}_3 & -\tilde{l}_{I_1O} & \boldsymbol{O}_{3\times3} & \boldsymbol{O}_{3\times3} \\
\boldsymbol{O}_{3\times3} & \boldsymbol{I}_3 & \boldsymbol{O}_{3\times3} & \boldsymbol{O}_{3\times3} \\
m\Omega^2\tilde{l}_{CO} & -\omega^2(m\tilde{l}_{I_1O}\tilde{l}_{I_1C}+\boldsymbol{J}_{I_1}) & \boldsymbol{I}_3 & \tilde{l}_{I_1O} \\
m\Omega^2\boldsymbol{I}_3 & -m\Omega^2\tilde{l}_{I_1C} & \boldsymbol{O}_{3\times3} & \boldsymbol{I}_3
\end{bmatrix}, \tag{14}
$$

$$
\boldsymbol{U}_{5,I_r} =
\begin{bmatrix}
\boldsymbol{O}_{3\times3} & \boldsymbol{O}_{3\times3} & \boldsymbol{O}_{3\times3} & \boldsymbol{O}_{3\times3} \\
\boldsymbol{O}_{3\times3} & \boldsymbol{O}_{3\times3} & \boldsymbol{O}_{3\times3} & \boldsymbol{O}_{3\times3} \\
\boldsymbol{O}_{3\times3} & \boldsymbol{O}_{3\times3} & \boldsymbol{I}_3 & \tilde{l}_{I_rO} \\
\boldsymbol{O}_{3\times3} & \boldsymbol{O}_{3\times3} & \boldsymbol{O}_{3\times3} & \boldsymbol{I}_3
\end{bmatrix} \quad (r=2,3), \tag{15}
$$

$$
\boldsymbol{H}_5 =
\begin{bmatrix}
\boldsymbol{I}_3 & \boldsymbol{O}_{3\times3} & \boldsymbol{O}_{3\times3} & \boldsymbol{O}_{3\times3} \\
\boldsymbol{O}_{3\times3} & \boldsymbol{I}_3 & \boldsymbol{O}_{3\times3} & \boldsymbol{O}_{3\times3}
\end{bmatrix}, \tag{16}
$$

$$
\boldsymbol{H}_{5,I_r} =
\begin{bmatrix}
\boldsymbol{I}_3 & \tilde{l}_{I_1I_r} & \boldsymbol{O}_{3\times3} & \boldsymbol{O}_{3\times3} \\
\boldsymbol{O}_{3\times3} & \boldsymbol{I}_3 & \boldsymbol{O}_{3\times3} & \boldsymbol{O}_{3\times3}
\end{bmatrix} \quad (r=2,3) \tag{17}
$$

where ω is the natural frequency of the IMU system, C denotes the center of mass, m is the mass of rigid body, $\boldsymbol{J}_I$ is moment of inertia matrix relative to the input point I_1, and $\tilde{l}_{I,O}$ are the cross product matrices from point I to point O.

Transfer equation and transfer matrix of elements 8. The transfer equation of elements 6~8 are

$$Z_{i,O} = U_i Z_{i,I} \ (i = 6, 7, 8). \tag{18}$$

The transfer matrices are

$$U_i = \begin{bmatrix} I_3 & O_{3\times3} & O_{3\times3} & U_{14} \\ O_{3\times3} & I_3 & U_{23} & O_{3\times3} \\ O_{3\times3} & O_{3\times3} & I_3 & O_{3\times3} \\ O_{3\times3} & O_{3\times3} & O_{3\times3} & I_3 \end{bmatrix} \ (i = 6, 7, 8), \tag{19}$$

where

$$U_{14} = \begin{bmatrix} -1/k_x & 0 & 0 \\ 0 & -1/k_y & 0 \\ 0 & 0 & -1/k_z \end{bmatrix}, \qquad U_{23} = \begin{bmatrix} 1/k'_x & 0 & 0 \\ 0 & 1/k'_y & 0 \\ 0 & 0 & 1/k'_z \end{bmatrix}.$$

Here k_x, k_y and k_z represent the stiffness coefficients of linear spring. k'_x, k'_y and k'_z denote the stiffness coefficients of rotary spring respectively.

Transfer equation and transfer matrix of elements 9~11. The gyros 9~11 are rigid bodies with single input and single output; their transfer equations are

$$Z_{i,O} = U_i Z_{i,I} \ (i = 9, 10, 11). \tag{20}$$

The transfer matrices are

$$U_i = \begin{bmatrix} I_3 & -\tilde{l}_{IO} & O_{3\times3} & O_{3\times3} \\ O_{3\times3} & I_3 & O_{3\times3} & O_{3\times3} \\ m\Omega^2\tilde{l}_{CO} & -\omega^2(m\tilde{l}_{IO}\tilde{l}_{IC} + J_I) & I_3 & \tilde{l}_{IO} \\ m\Omega^2 I_3 & -m\Omega^2\tilde{l}_{IC} & O_{3\times3} & I_3 \end{bmatrix} \ (i = 9, 10, 11). \tag{21}$$

4.3. *Overall transfer equation and overall transfer matrix of IMU system.* According to the automatic deduction theorem of overall transfer equation of multibody system [Yang et al. 2014], the overall transfer equation can be obtained as follows:

$$U_{all} Z_{all} = 0 \tag{22}$$

The overall transfer matrix is

$$U_{all} = \begin{bmatrix} -I_{12} & T_{9-1\sim4} & T_{10-1\sim4} & T_{11-1\sim4} \\ O_{6\times12} & G_{9-5} & G_{10-5} & O_{6\times12} \\ O_{6\times12} & G_{9-5} & O_{6\times12} & G_{11-5} \end{bmatrix}, \tag{23}$$

where

$$T_{9-1\sim4} = U_{1\sim4}U_5U_6U_9, \qquad G_{9-5} = -H_5U_6U_9,$$
$$T_{10-1\sim4} = U_{1\sim4}U_{5,7}U_7U_{10,}, \qquad G_{10-5} = H_{5,7}U_7U_{10},$$
$$T_{11-1\sim4} = U_{1\sim4}U_{5,8}U_8U_{11}, \qquad G_{11-5} = H_{5,8}U_8U_{11}.$$

Z_{all} is a column matrix consisting of the state vectors of system boundary points:

$$Z_{all} = [Z_{1\sim4,0}^T \quad Z_{9,0}^T \quad Z_{10,0}^T \quad Z_{11,0}^T]^T. \tag{24}$$

The boundary conditions of the system are

$$
\begin{aligned}
\boldsymbol{Z}_{1\sim4,0} &= [0 \quad 0 \quad 0 \quad 0 \quad 0 \quad 0 \quad M_x \quad M_y \quad M_z \quad Q_x \quad Q_y \quad Q_z]^{\mathrm{T}}_{1\sim4,0}, \\
\boldsymbol{Z}_{9,0} &= [X \quad Y \quad Z \quad \Theta_x \quad \Theta_y \quad \Theta_z \quad 0 \quad 0 \quad 0 \quad 0 \quad 0 \quad 0]^{\mathrm{T}}_{9,0}, \\
\boldsymbol{Z}_{10,0} &= [X \quad Y \quad Z \quad \Theta_x \quad \Theta_y \quad \Theta_z \quad 0 \quad 0 \quad 0 \quad 0 \quad 0 \quad 0]^{\mathrm{T}}_{10,0}, \\
\boldsymbol{Z}_{11,0} &= [X \quad Y \quad Z \quad \Theta_x \quad \Theta_y \quad \Theta_z \quad 0 \quad 0 \quad 0 \quad 0 \quad 0 \quad 0]^{\mathrm{T}}_{11,0}.
\end{aligned} \tag{25}
$$

Substituting the boundary conditions into (11) yields

$$
\bar{\boldsymbol{U}}_{all}\bar{\boldsymbol{Z}}_{\mathrm{all}} = \boldsymbol{0}, \tag{26}
$$

where $\bar{\boldsymbol{U}}_{\mathrm{all}}$ is a 24×24 square matrix composed of the 1st~6th, 19th~30th and 37th~42nd columns of $\boldsymbol{U}_{\mathrm{all}}$, $\bar{\boldsymbol{Z}}_{\mathrm{all}}$ is a column matrix consisting of the unknown elements in $\boldsymbol{Z}_{\mathrm{all}}$. For (20) to have nontrivial solutions, the determinant of its coefficient matrix must be zero, namely

$$
\det(\bar{\boldsymbol{U}}_{\mathrm{all}}) = 0. \tag{27}
$$

The eigenfrequencies ω_k $(k = 1, 2, 3, \ldots)$ of the IMU system can be obtained by solving (22). For each ω_k, using (20) and the transfer equations of elements, the state vector of any point can be got easily.

The body dynamics equations of IMU system can be written as

$$
\boldsymbol{M}_j\boldsymbol{v}_{j,tt} + \boldsymbol{C}_j\boldsymbol{v}_{j,t} + \boldsymbol{K}_j\boldsymbol{v}_j = \boldsymbol{f}_j, \tag{28}
$$

where j is the number of body element, the mass matrix $\boldsymbol{M}_j$ denotes the mass distribution of body element, displacement array $\boldsymbol{v}_j$ represents the motion state, consisting of the displacement and angular displacement variables of the body component and subscript t represents the time derivative time. The product of $\boldsymbol{K}_j$ and $\boldsymbol{v}_j$ represents all internal forces on the component and their action positions other than the damper force; $\boldsymbol{K}_j$ is called the stiffness parameter matrix; $\boldsymbol{C}_j$ acting on $\boldsymbol{v}_{j,t}$ represents the damping force on the body element and its action position, which is called a damping parameter matrix; $\boldsymbol{f}_j$ is the external force and torque of the body element. $\boldsymbol{f} = [\boldsymbol{f}_5^{\mathrm{T}} \quad \boldsymbol{f}_9^{\mathrm{T}} \quad \boldsymbol{f}_{10}^{\mathrm{T}} \quad \boldsymbol{f}_{11}^{\mathrm{T}}]^{\mathrm{T}}$; and $\boldsymbol{f}_j = [m_x, m_y, m_z, f_x, f_y, f_z]_j^{\mathrm{T}}$ is the column matrix of force (including torque) acted on the body j $(j = 5, 9, 10, 11)$.

4.4. *Power spectrum analysis method.* Using the modal superposition technology, the physical coordinates can be expanded in the form of augmented eigenvectors and generalized coordinates, i.e.,

$$
\boldsymbol{v}_j = \sum_{k=1}^{n} \boldsymbol{V}_j^k q^k(t). \tag{29}
$$

Substitute (29) into (28), make the inner product of $\boldsymbol{V}_j^k$ and sum up with j, then according to the orthogonality of the augmented eigenvector, it can be written as

$$
\ddot{q}^k(t) + \frac{\sum_j \left\langle \sum_{k=1}^{n} (\boldsymbol{C}_j\boldsymbol{V}_j^k)\dot{q}^k(t), \boldsymbol{V}_j^k \right\rangle}{d^k} + \omega_k^2 q^k(t) = \frac{\sum_j \langle \boldsymbol{f}_j, \boldsymbol{V}_j^k \rangle}{d^k} \tag{30}
$$

where

$$d^k = \sum_j \langle M_j V_j^k, V_j^k \rangle = \langle M_1 V_1^k, V_1^k \rangle + \langle M_3 V_3^k, V_3^k \rangle + \cdots\cdots + \langle M_{20} V_{20}^k, V_{20}^k \rangle,$$

$$\sum_j \langle f_j, V_j^k \rangle = \langle f_1, V_1^k \rangle + \langle f_3, V_3^k \rangle + \cdots\cdots + \langle f_{20}, V_{20}^k \rangle.$$

Then let

$$\frac{\sum_j \left\langle \sum_{k=1}^n (C_j V_j^k) \dot{q}^k(t), V_j^k \right\rangle}{d^k} = 2\zeta_k \omega_k. \tag{31}$$

Substituting (29) and (31) into (30), one obtains

$$\ddot{q}^k(t) + 2\zeta_k \omega_k \dot{q}^k(t) + \omega_k{}^2 q^k(t) = \omega_k^2 p^k(t), \tag{32}$$

where

$$p^k(t) = \frac{\sum_j \langle f_j, V_j^k \rangle}{\omega_k^2 d^k} = \frac{V^{k\mathrm{T}} f(t)}{\omega_k^2 d^k}. \tag{33}$$

Then $q^1, \ldots, q^n$ are calculated by means of numerical integration. The dynamic response of the isolation system can be obtained by substituting them into (29). If each component of $f(t)$ is a steady-state stochastic process, then the components of $v_j(t)$, $p^k(t)$, $q^k(t)$ are all steady-state stochastic processes. The correlation matrix of response v_j and generalized coordinates q^k are defined as

$$R_{v_j}(\tau) = \lim_{T \to \infty} \frac{1}{T} \int_{-T/2}^{T/2} v_j(t) v_j(t+\tau)^{\mathrm{T}} dt \tag{34}$$

$$R_{q^k}(\tau) = \lim_{T \to \infty} \frac{1}{T} \int_{-T/2}^{T/2} q^k(t) q^k(t+\tau)^{\mathrm{T}} dt, \tag{35}$$

$$R_q(\tau) = \lim_{T \to \infty} \frac{1}{T} \int_{-T/2}^{T/2} q(t) q(t+\tau)^{\mathrm{T}} dt = \begin{bmatrix} R_{q^1} & \cdots & R_{q^1 q^k} & \cdots & R_{q^1 q^n}, \\ \vdots & \ddots & & & \\ R_{q^k q^1} & & R_{q^k} & & R_{q^k q^n} \\ \vdots & & & \ddots & \\ R_{q^n q^1} & \cdots & R_{q^n q^k} & \cdots & R_{q^n} \end{bmatrix}. \tag{36}$$

According to (36), this yields

$$R_{v_j}(\tau) = V_j R_q(\tau) V_j{}^{\mathrm{T}}. \tag{37}$$

The correlation matrices of generalized force p and external force f are

$$R_{p^k}(\tau) = \lim_{T \to \infty} \frac{1}{T} \int_{-T/2}^{T/2} p^k(t) p^k(t+\tau)^{\mathrm{T}} dt, \qquad R_f(\tau) = \lim_{T \to \infty} \frac{1}{T} \int_{-T/2}^{T/2} f(t) f(t+\tau)^{\mathrm{T}} dt, \tag{38}$$

Then one gets

$$R_{p^k}(\tau) = \frac{V^{k\mathrm{T}} R_f(\tau) V^k}{\omega_k^4 d^{k2}}, \quad k = 1, \ldots, n, \qquad R_{p^r p^s}(\tau) = \frac{V^{r\mathrm{T}} R_f(\tau) V^s}{\omega_r^2 \omega_s^2 d^r d^s}, \quad r, s = 1, \ldots, n, \ r \neq s. \tag{39}$$

The power spectral matrix is deduced by Fourier transformation of the correlation matrix of the response in physical coordinates

$$S_{v_j}(\omega) = \int_{-\infty}^{+\infty} \boldsymbol{R}_{v_j}(\tau) e^{-i\omega\tau} d\tau \tag{40}$$

The transformation relationships between $\boldsymbol{S}_{v_j}(\omega)$ and $\boldsymbol{S}_q(\omega)$, $S_{p^k}(\omega)$ and $\boldsymbol{S}_f(\omega)$ can be obtained as

$$\boldsymbol{S}_{v_j}(\omega) = \boldsymbol{V}_j \boldsymbol{S}_q(\omega) \boldsymbol{V}_j^{\mathrm{T}}, \qquad S_{p^k}(\omega) = \frac{\boldsymbol{V}^{k\mathrm{T}} \boldsymbol{S}_f(\omega) \boldsymbol{V}^k}{\omega_k^4 d^{k2}}, \quad k = 1, \ldots, n, \tag{41}$$

$$S_{p^r p^s}(\omega) = \frac{\boldsymbol{V}^{r\mathrm{T}} \boldsymbol{S}_f(\omega) \boldsymbol{V}^s}{\omega_r^2 \omega_s^2 d^r d^s}, \quad r, s = 1, \ldots, n. \tag{42}$$

Taking the Laplace transform of (32) and substituting $s = j\omega$, one gets

$$H^k(\omega) = \frac{q^k(\omega)}{p^k(\omega)} = \frac{\omega_k^2}{\omega_k^2 - \omega^2 + 2\zeta_k \omega_k j\omega}, \quad k = 1, \ldots, n, \tag{43}$$

$$S_{q^k}(\omega) = H^{k^*}(\omega) S_{p^k}(\omega) H^k(\omega), \qquad k = 1, \ldots, n, \tag{44}$$

where $H^{k^*}(\omega)$ is the conjugate function of $H^k(\omega)$. The relationships between the power spectra of system output in physical coordinate and system physical force are as follows:

$$S_{p^k}(\omega) = \frac{\boldsymbol{V}^{k\mathrm{T}} \boldsymbol{S}_f(\omega) \boldsymbol{V}^k}{\omega_k^4 d^{k2}}, \qquad k = 1, \ldots, n, \tag{45}$$

$$S_{p^r p^s}(\omega) = \frac{\boldsymbol{V}^{r\mathrm{T}} \boldsymbol{S}_f(\omega) \boldsymbol{V}^s}{\omega_r^2 \omega_s^2 d^r d^s}, \qquad r, s = 1, \ldots, n, \tag{46}$$

$$S_{q^k}(\omega) = H^{k^*}(\omega) S_{p^k}(\omega) H^k(\omega), \qquad k = 1, \ldots, n, \tag{47}$$

$$S_{q^r q^s}(\omega) = H^{r^*}(\omega) S_{p^r p^s}(\omega) H^s(\omega), \quad r, s = 1, \ldots, n, r \neq s, \tag{48}$$

$$\boldsymbol{S}_q(\omega) = \begin{bmatrix} S_{q^1} & \cdots & S_{q^1 q^k} & \cdots & S_{q^1 q^n} \\ \vdots & \ddots & & & \\ S_{q^k q^1} & & S_{q^k} & & S_{q^k q^n} \\ \vdots & & & \ddots & \\ S_{q^n q^1} & \cdots & S_{q^n q^k} & \cdots & S_{q^n} \end{bmatrix}, \tag{49}$$

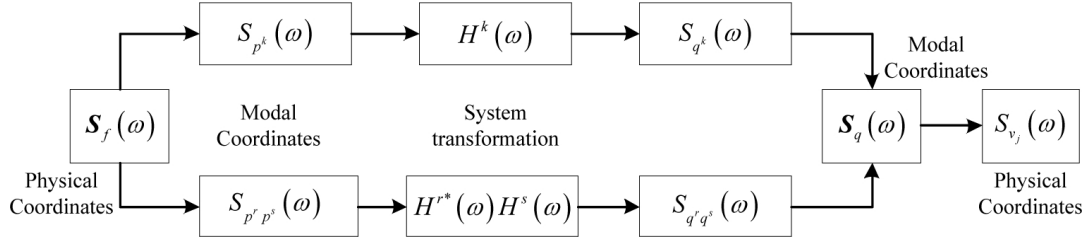$$\boldsymbol{S}_{v_j}(\omega) = \boldsymbol{V}_j \boldsymbol{S}_q(\omega) \boldsymbol{V}_j^{\mathrm{T}}. \tag{50}$$

The correlation function of the response power spectrum is

$$\boldsymbol{R}_{v_j}(\tau) = \frac{1}{2\pi} \int_{-\infty}^{+\infty} \boldsymbol{S}_{v_j}(\omega) e^{i\omega\tau} d\omega. \tag{51}$$

Let $\tau = 0$. The root mean square (RMS) σ_{v_j} of the response v_j is

$$\sigma_{v_j}^2 = \boldsymbol{R}_{v_j}(0) = \frac{1}{2\pi} \int_{-\infty}^{+\infty} \boldsymbol{S}_{v_j}(\omega) d\omega. \tag{52}$$

Figure 13. Transformation flow of PSD.

The transformation flow of PSD is shown in Figure 13.

According to the displacement PSD in physical coordinates, the velocity and acceleration PSD in physical coordinates can be obtained:

$$S_{\dot{v}_j}(\omega) = \omega^2 S_{v_j}(\omega), \tag{53}$$

$$S_{\ddot{v}_j}(\omega) = \omega^4 S_{v_j}(\omega). \tag{54}$$

When frequency is expressed in Hz, the relationship between the power spectra is described by

$$S_{v_j}(f) = 2\pi S_{v_j}(\omega). \tag{55}$$

5. Simulation results and analysis

It is supposed that the random vibration as input is a stationary Gauss process $\ddot{y}(t)$. The sampling function of $\ddot{y}(t)$ can be written approximately as Fourier series $\ddot{y}^d(t)$:

$$\ddot{y}^d(t) = \sum_{k=1}^{N} a_k \cos(\omega_k t + \varphi_k), \tag{56}$$

where the phase angle φ_k is an independent random variable with range $[0, 2\pi]$. The amplitude a_k is

$$a_k^2 = 4 S_{\ddot{y}}(\omega_k) \Delta\omega, \tag{57}$$

where $S_{\ddot{y}}(\omega)$ is the input PSD, $\Delta\omega = (\omega_u - \omega_l)/N$, ω_u and ω_l are frequency upper limit and lower limit value for input PSD. The frequency ω_k can be written as
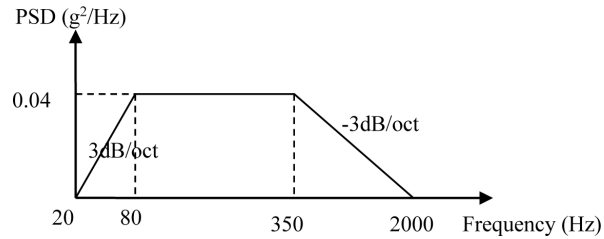
$$\omega_k = \omega_l + (k - 1/2)\Delta\omega, \quad k = 1, 2, \ldots, N. \tag{58}$$

Equation (56) presents a stationary and ergodic Gaussian random process. The mean value is

$$E(\ddot{y}^d(t)) = \lim_{T \to \infty} \frac{1}{T} \sum_{k=1}^{N} a_k \int_0^T \cos(\omega_k t + \varphi_k)\, dt = 0. \tag{59}$$

The autocorrelation function is

$$\varphi_{\ddot{y}}^d(\tau) = \lim_{T \to \infty} \frac{1}{T} \int_0^T \ddot{y}^d(t)\ddot{y}^d(t + \tau)dt = \frac{1}{2} \sum_{k=1}^{N} a_k^2 \cos \omega_k \tau. \tag{60}$$

Figure 14. PSD of input acceleration.

The PSD of input acceleration is shown in Figure 14 with RMS value of 6.7 g. The input displacement and velocity time history is illustrated in Figure 15. Figure 16 demonstrates the theoretical simulation results for the displacement curve of payload when the MRE isolator is applied with a series of constant currents. The RMS values of payload with different currents are listed in Table 2 on page 582. It can be seen that with the increasing current, the RMS of displacement decreases and acceleration increases.
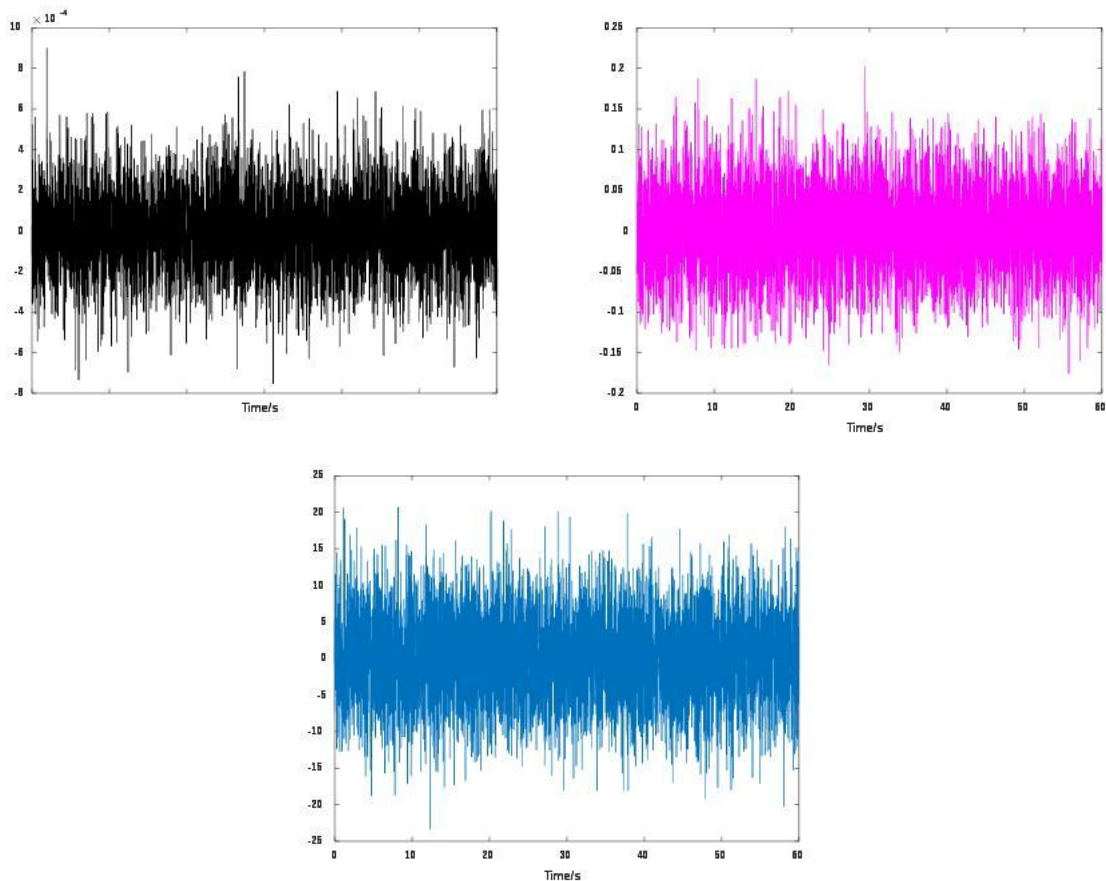

Figure 15. Input signals in time domain: displacement (top left), velocity (top right) and acceleration (bottom).
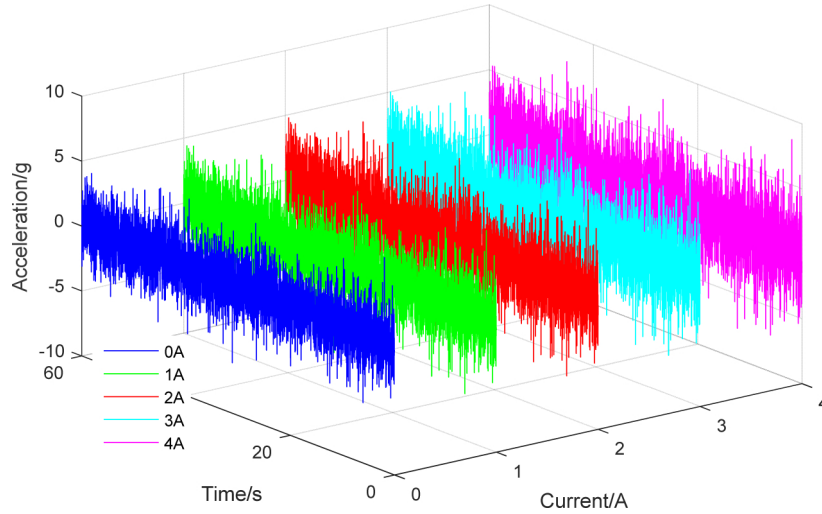
Figure 16. Acceleration of payload with a series of constant currents.

The changes of RMS values of displacement and acceleration are 11.38% and 39.71%, respectively. Figure 17 shows the PSD of the acceleration for payload when the MRE isolator is applied with a series of constant currents. The peak value of PSD is $1.07\,\text{g}^2/\text{Hz}$ at 0.0 A. The peak value of PSD decreases by 48.8% when current is increased from 0.0 A to 4.0 A. The minimal root mean square value is 2.97 g when the current is 4.0 A. The resonance peak apparently shifts with the increasing current. The natural frequency change of a SDOF system is affected by changing the MRE isolator stiffness. These changes indicate that it is possible to control MRE isolator over varying stiffness and damping.
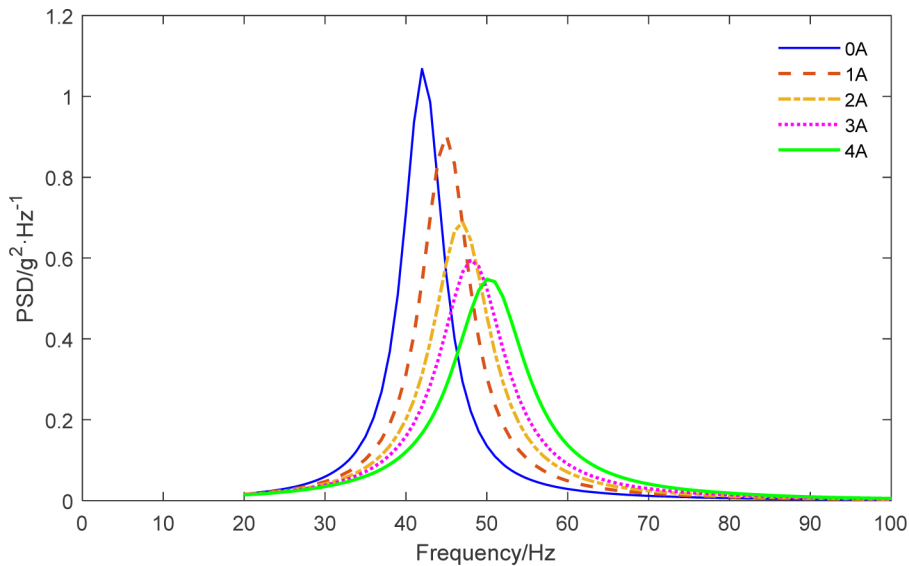
Figure 17. PSD of the payload acceleration with a series of constant currents.

root mean square	current/A					change
	0	1	2	3	4	
displacement/m	$5.91 \cdot 10^{-5}$	$5.79 \cdot 10^{-5}$	$5.47 \cdot 10^{-5}$	$5.32 \cdot 10^{-5}$	$5.24 \cdot 10^{-5}$	-11.38%
velocity/(m/s)	0.016	0.016	0.016	0.016	0.016	5.10%
acceleration/g	1.43	1.63	1.77	1.87	2.00	39.73%

Table 2. RMS values of payload with a series of constant currents.

6. Conclusions

This paper reports the design, fabrication, experimental tests and model simulation of the compression MRE isolator. The experimental results of MRE isolator exhibit that both its stiffness and the damping ratio are controllable with input currents. The simulation results show that the peak of PSD is reduced with increasing input current under random input vibration. Thus, it is demonstrated that the MRE isolator, whose mechanical properties can be controlled by an applied magnetic field, has potential applications where tuning vibration characteristics are desired.

Acknowledgements

References

[Behrooz et al. 2014] M. Behrooz, X. Wang, and F. Gordaninejad, "Performance of a new magnetorheological elastomer isolation system", *Smart Mater. Struct.* **23**:4 (2014), art. id. 045014.

[Brancati et al. 2017] R. Brancati, G. Di Massi, and S. Pagano, "A vibration isolator based on magneto-rheological elastomer", pp. 483–490 in *Advances in Italian mechanism science* (Vincenza, Italy, 2016), edited by G. Boschetti and A. Gasparetto, Mech. Mach. Sci. **47**, Springer, 2017.

[Chen et al. 2013] G. Chen, X. Rui, F. Yang, J. Zhang, and Q. Zhou, "Study on the dynamics of laser gyro strapdown inertial measurement unit system based on transfer matrix method for multibody system", *Adv. Mech. Eng.* **5** (2013), art. id. 854583.

[Deng et al. 2006] H.-x. Deng, X.-l. Gong, and L.-h. Wang, "Development of an adaptive tuned vibration absorber with magnetorheological elastomer", *Smart Mater. Struct.* **15**:5 (2006), N111–N116.

[Dong et al. 2009] X.-m. Dong, M. Yu, C.-r. Liao, and W.-m. Chen, "A new variable stiffness absorber based on magnetorheological elastomer", *Trans. Nonferr. Met. Soc. China* **19**:suppl. 3 (2009), S611–S615.

[Ginder et al. 2000] J. M. Ginder, M. E. Nichols, L. D. Elie, and S. M. Clark, "Controllable-stiffness components based on magnetorheological elastomers", pp. 418–425 in *Smart structures and materials* (Newport Beach, CA, 2000), edited by N. M. Wereley, Proc. SPIE **3985**, SPIE, Bellingham, WA, 2000.

[Kallio 2005] M. Kallio, "The elastic and damping properties of magnetorheological elastomers", technical report 565, Department of Materials Science, Tampere University of Technology, Finland, 2005.

[Liao et al. 2012] G. J. Liao, X.-L. Gong, S. H. Xuan, C. J. Kang, and H. Zong, "Development of a real-time tunable stiffness and damping vibration isolator based on magnetorheological elastomer", *J. Intell. Mater. Syst. Struct.* **23**:1 (2012), 25–33.

[Liu 2012] X. Liu, *Magnetorheological elastomer isolator in shear-compression mixed mode*, master's thesis, Chongqing University, 2012.

[Tao et al. 2019] Y. Tao, X. Rui, F. Yang, and B. Hao, "Development of a MRE isolation system for strapdown inertial measurement unit", *Mech. Syst. Signal Process.* **117** (2019), 553–568.

[Yang et al. 2014] F. Yang, X. Rui, Z. Song, and G. Chen, "Vibration effects analysis of IMU by transfer matrix method for multibody system", pp. 101–106 in *Proceedings of the Fifth International Conference on Mechanical Engineering and Mechanics* (Jiangsu, China, 2014), China Acad. J. Elect. Publ., Beijing, 2014.

[Yang et al. 2016] J. Yang, S. Sun, T. Tian, W. Li, H. Du, G. Alici, and M. Nakano, "Development of a novel multi-layer MRE isolator for suppression of building vibrations under seismic events", *Mech. Syst. Signal Process.* **70-71** (2016), 811–820.

YANG FUFENG: fufengyang@aliyun.com
, *Nanjing University of Science and Technology, 200 Xiaoling Wei Street, Jiangsu Province, Nanjing, 210094, China*

TAO YU: shirleyo0o@163.com
, *Xi'an Technological University, 2 Xuefu Middle Road, Weiyang District, Shaanxi Province, Xi'an, 710021, China*